LncRNA Uc003xsl.1-Mediated Activation of the NFκB/IL8 Axis Promotes Progression of Triple-Negative Breast Cancer

Ying Xu[1,2,3,4,5], Wei Ren[3,5], Qingjian Li[1,2,3,5], Chaohui Duan[1,2,4,5], Xiaorong Lin[1,2,5], Zhuofei Bi[1,2,3,5], Kaiyun You[1,2,3,5], Qian Hu[3,5], Ning Xie[3,5], Yunfang Yu[1,2,3,5], Xiaoding Xu[1,2,5], Hai Hu[1,2,3,5], and Herui Yao[1,2,3,5,6]

ABSTRACT

Aberrant activation of NFκB orchestrates a critical role in tumor carcinogenesis; however, the regulatory mechanisms underlying this activation are not fully understood. Here we report that a novel long noncoding RNA (lncRNA) Uc003xsl.1 is highly expressed in triple-negative breast cancer (TNBC) and correlates with poor outcomes in patients with TNBC. Uc003xsl.1 directly bound nuclear transcriptional factor NFκB-repressing factor (NKRF), subsequently preventing NKRF from binding to a specific negative regulatory element in the promoter of the NFκB-responsive gene *IL8* and abolishing the negative regulation of NKRF on NFκB-mediated transcription of IL8. Activation of the NFκB/IL8 axis promoted the progression of TNBC. Trop2-based antibody–drug conjugates have been applied in clinical trials in TNBC. In this study, a Trop2-targeting, redox-responsive nanoparticle was developed to systematically deliver Uc003xsl.1 siRNA to TNBC cells *in vivo*, which reduced Uc003xsl.1 expression and suppressed TNBC tumor growth and metastasis. Therefore, targeting Uc003xsl.1 to suppress the NFκB/IL8 axis represents a promising therapeutic strategy for TNBC treatment.

Significance: These findings identify an epigenetic-driven NFκB/IL8 cascade initiated by a lncRNA, whose aberrant activation contributes to tumor metastasis and poor survival in patients with triple-negative breast cancer.

Introduction

Triple-negative breast cancer (TNBC), which accounted for 10%–20% of invasive breast cancer cases, is characterized by significant heterogeneity and poor prognosis (1). Tumor metastasis is the leading cause of treatment failure and death in patients with TNBC (2). Therefore, understanding the mechanisms of TNBC metastasis and exploring the targeting strategy is an urgent requirement. Long noncoding RNAs (lncRNA) are involved in regulating critical hallmarks of cancer, including proliferation (3, 4), viability (5, 6), and metastasis (7, 8), suggesting that lncRNAs represent novel biomarkers and therapeutic targets of TNBC. Previous studies show that lncRNAs specifically interact with proteins, including epigenetic modifiers (9), transcriptional factors/coactivators (10, 11), and RNP complexes (12), to exert their regulatory functions. However, the regulatory mechanisms of lncRNAs in TNBC metastasis remain poorly understood.

The aberrant activation of NFκB, consisting of a family of transcription factors that orchestrate critical biological processes in the inflammatory response, cell proliferation, differentiation, and survival (13), has been observed in various types of breast cancers, including TNBC (14, 15). Aberrant NFκB activation, a consequence of fostering an inflammatory milieu in which various cytokines aid and abet malignant transformation (16), plays a critical role in initiating and promoting cancer (17, 18). In the current study, we revealed a novel mechanism of lncRNA to regulate the transcriptional activation of the NFκB pathway and TNBC progression.

A novel lncRNA (Uc003xsl.1) was upregulated in TNBC tissues and served as an independent predictor for the prognosis of patients with TNBC. Mechanistically, Uc003xsl.1 directly interacts with a nuclear transcriptional factor NFκB-repressing factor (NKRF) in the nucleus, which could subsequently prevent NKRF from acting as the negative regulator of NFκB-mediated transcription, especially for IL8 transcription. This activated cascade of the NFκB/IL8 axis promotes the progression of TNBCs. Trop2 based antibody–drug conjugates have been applied in clinical trials in TNBCs and other solid tumors (NCT04152499, NCT04601285). On the basis of the above regulatory mechanism, a Trop2-targeting redox-responsive nanoparticle (NP) system was developed to systematically deliver Uc003xsl.1 siRNA to TNBC tumor *in vivo*, which further improved the therapeutic effect of Uc003xsl.1-targeting NP against TNBCs.

[1]Guangdong Provincial Key Laboratory of Malignant Tumor Epigenetics and Gene Regulation, Medical Research Center, Sun Yat-sen Memorial Hospital, Sun Yat-sen University, Guangzhou, P.R. China. [2]RNA Biomedical Institute, Sun Yat-sen Memorial Hospital, Sun Yat-sen University, Guangzhou, P.R. China. [3]Department of Oncology, Sun Yat-sen Memorial Hospital, Sun Yat-sen University, Guangzhou, P.R. China. [4]Department of Clinical Laboratory, Sun Yat-sen Memorial Hospital, Sun Yat-sen University, Guangzhou, P.R. China. [5]Center for Precision Medicine, Sun Yat-sen University, Guangzhou, P.R. China. [6]Breast Tumor Center, Sun Yat-sen Memorial Hospital, Sun Yat-sen University, Guangzhou, P.R. China.

Note: Supplementary data for this article are available at Cancer Research Online (http://cancerres.aacrjournals.org/).

Y. Xu, W. Ren, Q. Li, and C. Duan contributed equally to this article.

Corresponding Authors: Herui Yao, Department of Oncology, Sun Yat-sen Memorial Hospital, Sun Yat-sen University, 107 Yanjiang West Road, Guangzhou 510120, P.R. China. Phone: 8620-8133-2182; Fax: 8620-8133-2853; E-mail: yaoherui@mail.sysu.edu.cn; Hai Hu, huhai@mail.sysu.edu.cn; and Xiaoding Xu, xuxiaod5@mail.sysu.edu.cn

Cancer Res 2022;82:556–70

doi: 10.1158/0008-5472.CAN-21-1446

Materials and Methods

Patients and clinical samples

Tumors and adjacent breast cancer tissues were obtained from patients who underwent surgery at the Breast Tumor Center, Sun Yat-sen Memorial Hospital, Sun Yat-sen University (Guangzhou, P.R. China), from January 2012 to December 2015. None of these patients received radiotherapy or chemotherapy prior to surgery. Pathologic diagnosis and estrogen receptor/PR and Her2 status were verified by two separate pathologists. All samples were collected with informed written consent from patients. All related procedures were performed with the approval of the Institutional Review Board of the Sun Yat-sen Memorial Hospital (Guangzhou, P.R. China).

RNA pulldown assay

The full-length sense and antisense of Uc003xsl.1 were prepared by *in vitro* transcription using MEGAscriptT7 Transcription kit (Invitrogen) and were labeled with Bio-16-UTP(Invitrogen)and purified with a Gene JET RNA Purification Kit (Thermo Fisher Scientific). The RNA pulldown assay was performed with a Pierce Magnetic RNA-Protein PullDown Kit (Thermo Fisher Scientific) following the manufacturer's instructions.

RNA-binding protein immunoprecipitation

A total of 5×10^6–1×10^7 cells transfected with siRNAs or plasmids were collected, lysed with lysis buffer containing 1 mL Pierce immunoprecipitation (IP) lysis buffer (Thermo Fisher Scientific), 10 μL Halt Protease Inhibitor (Thermo Fisher Scientific), and 10 μL EDTA (Thermo Fisher Scientific), and incubated on ice for 30 minutes, followed by centrifugation at 16,000 $\times g$ for 20 minutes to collect the supernatant. Then, 50 μL (10%) of the supernatant was removed as "input," and the remaining was divided into two parts: one was incubated with target antibodies and the other with a negative control normal rabbit IgG at 4°C overnight with rotation. Next, 20 μL Protein A Dynabeads beads (Thermo Fisher Scientific) was added to "Target" IP and "IgG" IP complex for 2 hours at room temperature with rotation. Then RNA was extracted from the Protein A bead–antibody/chromatin complex and "input" lysis. Retrieved RNA was subjected to qRT-PCR analysis. Normal IgG was utilized as a negative control.

Chromatin immunoprecipitation assay

About 5×10^6–1×10^7 cells transfected with siRNAs or plasmids were collected and cross-linked in 1% formaldehyde solution for 10 minutes at room temperature, followed by the addition of 125 mmol/L glycine for 5 minutes. Chromatin immunoprecipitation (ChIP) assay was performed with an EZ-Magna ChIP Kit (Merck Millipore), following the manufacturer's instructions. The nuclear lysis was sheared to yield DNA fragments ranging from 100–500 bp by a sonication system-Bioruptor (Diagenode). Two micrograms of normal IgG were used as the negative control, anti-NKRF (ab168829, Abcam) and anti-P65 (8244, Cell Signaling Technology) were used for each immunoprecipitation. The IPs were eluted and reverse cross-linked, after which, the DNA fragments were purified. Immunoprecipitated and input DNAs were subjected to qRT-PCR analysis. The primers used for amplifying the IL8 promoter region spanning the NKRF-binding site were forward: 5′-GGTTTGCCCTGAGGGGATGG-3′ and reverse: 5′-CTTGTGTGCTCTGCTGTCTCT-3′. The immunoprecipitated DNA was further analyzed by ChIP-PCR and ChIP coupled with high-throughput sequencing (ChIP-seq).

Tumor xenografts

Female nude mice (4–6 weeks old) were bred and maintained under specific pathogen-free barrier facilities at the Animal Experiment Center of Sun Yat-sen University. All procedures were approved by the Institutional Animal Care and Use Committee of Sun Yat-sen University and conformed to the legal mandates and national guidelines for the care and maintenance of laboratory animals. The detailed methods of xenografts are described in the Supplementary Data.

Statistical analysis

All statistical analyses were performed using SPSS 13.0 software (IBM, SPSS). Two-tailed Student *t* tests were utilized for comparisons between two groups. One-way ANOVA with Bonferroni test was utilized for multiple comparisons. The overall survival (OS) and disease-free survival (DFS) were calculated using the Kaplan–Meier method with the log-rank test. Multivariate Cox regression analysis was used to evaluate the survival data. A $P < 0.05$ was considered statistically significant.

Data availability

The sequence data of lncRNA Uc003xsl.1 are publicly available in GenBank at MW417110. Expression profile data of the RNA sequencing (RNA-seq) and ChIP-seq analyzed in this study are available in Gene Expression Omnibus at GSE163953, and within the article and its Supplementary Data files.

Results

Highly expressed Uc003xsl.1 is correlated with metastasis and the poor outcomes of TNBCs

To discover the potential drivers of TNBC metastasis, we established an *in vivo* model by injecting MDA-MB-231cells into the tail veins of mice. Then, the breast tumor cells that successfully grew into metastatic lung tumors were collected and expanded *in vitro*, followed by reinjection into the tail veins of mice for lung metastasis. After three rounds of selection, a highly metastatic subline, MDA-MB-231-P3, was established (Supplementary Fig. S1A), and more frequent micrometastasis was detected in MDA-MB-231-P3 groups than that of MDA-MB-231 groups after hematoxylin and eosin (H&E) staining of the mice lungs (Supplementary Fig. S1B). The lncRNA profiles of MDA-MB-231 or MDA-MB-231-P3 cells were analyzed by lncRNA sequencing. A total of 267 lncRNAs in MDA-MB-231-P3 cells were upregulated more than 2-fold compared with the MDA-MB-231 cells (**Fig. 1A**; Supplementary Table S1). To further identify which of these lncRNAs were specifically involved in TNBC-related metastasis machinery, we also compared the lncRNA profiles of TNBC tumor tissues with that of luminal breast tumor tissues (**Fig. 1B**; Supplementary Table S2). Then, the lncRNAs, MIF-AS1, PRNCR1, and Uc003xsl.1, were also highly expressed in TNBCs compared with those of luminal tumors and were selected for further exploration (**Fig. 1C**). Among these candidate lncRNAs, Uc003xsl.1 was overexpressed approximately 4-fold in both TNBC cancer tissues and the highly metastatic MDA-MB-231-P3 cells relative to control tissue or cells by qRT-PCR validation (**Fig. 1D** and **E**). However, the fold change of Uc003xsl.1 expressions between MDA-MB-231-P3 and parental MDA-MB-231 cells did not have a significant P_{adj} in initial RNA-seq datasets (Supplementary Table S1), which may be due to the small number of replicates in the RNA-seq assay. So, the expression of Uc003xsl.1 was further validated in 50 breast cancer tissues (cohort 1). qRT-PCR revealed that Uc003xsl.1 was highly expressed in TNBC cancer tissues compared with the other subtype of breast cancers

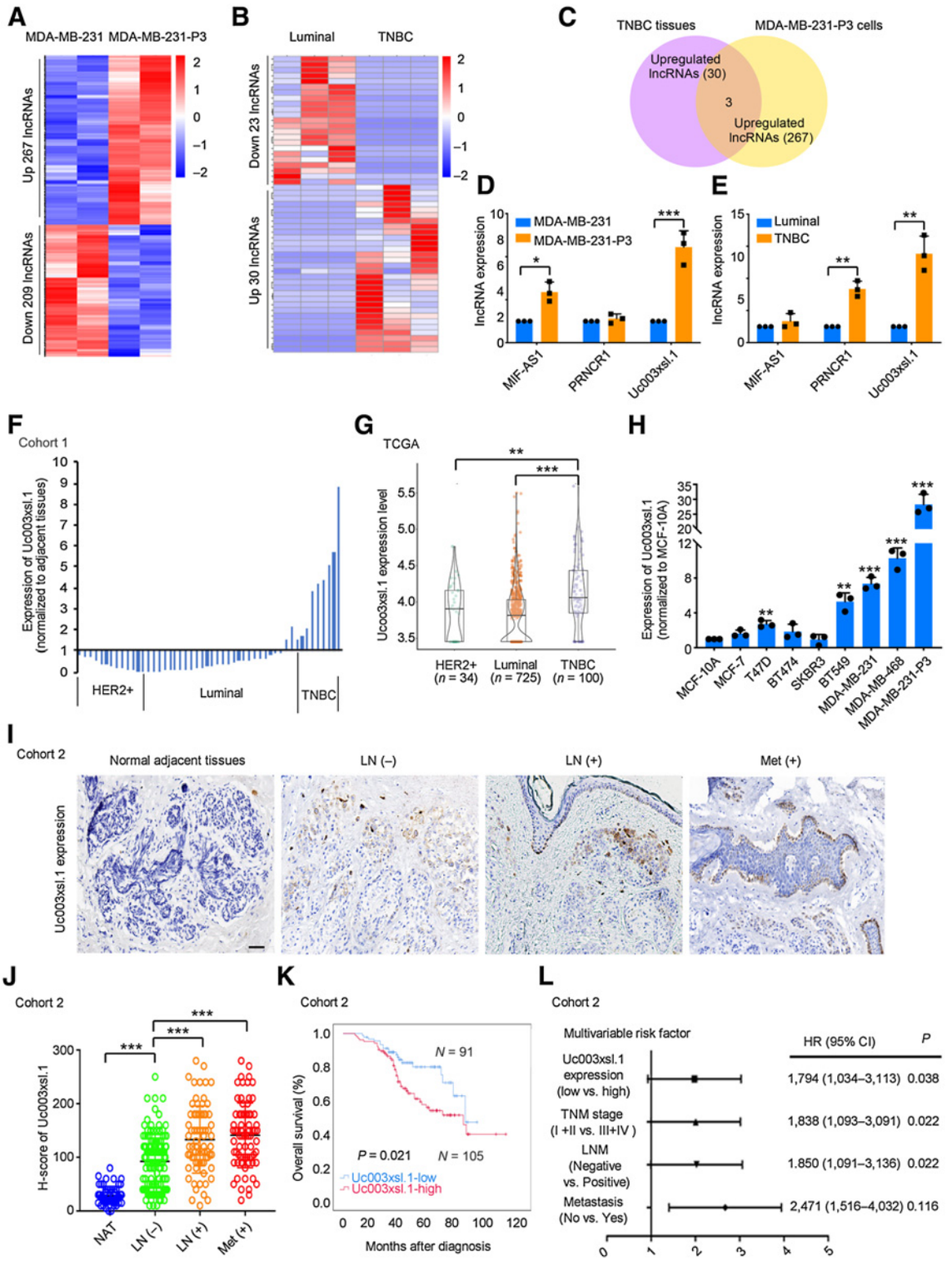

Figure 1.

High expression of Uc003xsl.1 predicts poor clinical outcomes in patients with TNBC. **A,** RNA-seq analysis revealed that lncRNA was differentially expressed in highly metastatic MDA-MB-231-P3 cells and MDA-MB-231 cells. **B,** RNA-seq analysis revealed that lncRNAs are differentially expressed in six breast tumor tissues, including three luminal cases and three TNBC cases. **C,** The number of overlapped lncRNAs upregulated in TNBC tumor tissues and MDA-MB-231-P3 cells. **D** and **E,** The expression of overlapped lncRNAs upregulated in highly metastatic MDA-MB-231-P3 cells (**D**) and TNBC tumor tissues (**E**) was verified by qRT-PCR. **F,** Uc003xsl.1 expression in fresh human breast tumor tissues ($n = 50$, cohort 1) paired with normal adjacent tissues was detected by qRT-PCR. Uc003xsl.1 levels in TNBC tissues were significantly higher than those in other subtypes of breast cancer. (*Continued on the following page.*)

(**Fig. 1F**), which was consistent with the analysis using The Cancer Genome Atlas (TCGA; **Fig. 1G**; Supplementary Table S3). In agreement with these observations, Uc003xsl.1 showed the highest expression in highly metastatic MDA-MB-231-P3 cells and TNBC cell lines (MDA-MB-468, MDA-MB-231, and BT549 cells) than other subtype breast cancer cell lines (**Fig. 1H**). These results implied that Uc003xsl.1 might be involved in TNBC-related metastasis.

Uc003xsl.1 expression was further evaluated by ISH in 196 paraffin-embedded TNBC tissues and 60 normal adjacent tissues (cohort2; **Fig. 1I**; Supplementary Table S4), which revealed significantly increased Uc003xsl.1 level in TNBC tissues compared with the normal adjacent tissues (Supplementary Fig. S1C). In addition, elevated Uc003xsl.1 was associated with advanced tumor–node–metastasis stage, lymph node (LN) metastasis, or positive distant metastasis (**Fig. 1J**; Supplementary Fig. S1D; Supplementary Table S5) and correlated with shorter OS and DFS (**Fig. 1K**; Supplementary Fig. S1E). Multivariate regression analysis (Cox proportional hazards regression model) further revealed that Uc003xsl.1 level was an independent predictor for OS in patients with TNBC ($P = 0.038$; **Fig. 1L**; Supplementary Table S6). In conclusion, the high expression of Uc003xsl.1 is associated with metastasis and poor outcome of TNBCs.

Uc003xsl.1 promotes TNBCs progression *in vitro* and *in vivo*

Full-length Uc003xsl.1 (1,905 bp) was identified using the 5′ and 3′ rapid amplification of cDNA ends PCR (Supplementary Fig. S2A; Supplementary Table S7). Analysis using ORF Finder from the National Center for Biotechnology Information did not identify any potential protein-encoding segments within the Uc003xsl.1 sequence (Supplementary Fig. S2B). FISH displayed that Uc003xsl.1 was predominantly localized in the nucleus (Supplementary Fig. S2C). This finding was further confirmed by nuclear/cytoplasm fractionation (Supplementary Fig. S2D and S2E). Collectively, Uc003xsl.1 is a novel lncRNA with a full length of 1,905 bp and is mainly localized in the nucleus of TNBC cells.

Next, we examined the role of Uc003xsl.1 in TNBC progression. siRNA-mediated knockdown and plasmid-mediated overexpression were used for exogenous manipulation of Uc003xsl.1 expression (**Fig. 2A** and **B**) in TNBC cells. The knockdown of Uc003xsl.1 inhibited the growth of MDA-MB-231-P3 (**Fig. 2C**). Similarly, silencing Uc003xsl.1 results in reduced EdU incorporation, supporting slow cell proliferation (Supplementary Fig. S2F). In addition, transwell assays displayed that the knockdown of Uc003xsl.1 inhibited MDA-MB-231-P3 cells migration and invasion (**Fig. 2E** and **G**). On the other hand, overexpression of Uc003xsl.1 in BT549 cells promoted cell proliferation (**Fig. 2D**; Supplementary Fig. S2G) and boosted cell migration and invasion (**Fig. 2F** and **H**). Moreover, overexpression of Uc003xsl.1 in parental MDA-MB-231 cells to the level of that in MDA-MB-231-P3 cells enhanced cell proliferation, migration, and invasion ability similarly to the phenotypes of MDA-MB-231-P3 cells (Supplementary Fig. S3A, S3C, S3E, and S3G). The level of Uc003xsl.1 in MDA-MB-468 cells was higher than in MDA-MB-231 and BT549 cells (**Fig. 1H**). Thus, the function of endogenous Uc003xsl.1 was also assessed in MDA-MB-468 cells. We found that knockdown of Uc003xsl.1 in MDA-MB-468 cells reduced cell proliferation, migration, and invasion (Supplementary Fig. S3B, S3D, S3F, and S3H). These data showed that Uc003xsl.1 might promote TNBC progression by regulating cancer cell proliferation and metastasis.

To further assess the oncogenic roles of Uc003xsl.1 in TBNC progression, the xenograft TNBC model was used. MDA-MB-231-P3 cells with stable expression of sh-Uc003xsl.1 (sh-lnc1 and sh-lnc2) or sh-control (sh-NC) were injected into the left armpits of nude mice for the formation of TNBC xenografts. Uc003xsl.1 knockdown markedly suppressed the tumor growth (**Fig. 2I–K**). To evaluate the role of Uc003xsl.1 in promoting TNBC metastasis, a lung metastatic model was used. MDA-MB-231-P3 cells with luciferase expression were injected into the tail veins of mice for lung metastasis. After 7 weeks post-injection, the gross lung images showed that fewer metastatic foci on the lung surface of Uc003xsl.1 knocked down groups (**Fig. 2L** and **M**). We also found fewer micrometastatic loci in the lung of Uc003xsl.1 knockdown group when the mice lung sections were stained by H&E (**Fig. 2L**). These data suggested that the overexpression of Uc003xsl.1 promotes TNBC progression by increasing breast cancer cell proliferation and metastasis.

Uc003xsl.1 binds NKRF to promote TNBC progression

lncRNAs modulate signal transduction or transcription by directly interacting with key proteins in these processes (19). To elucidate Uc003xsl.1-mediated progression of TNBC, we identified Uc003xsl.1-binding proteins using RNA pulldown assay with nuclear extracts of MDA-MB-231-P3 cells. A 70-kDa protein showed specific binding with Uc003xsl.1 (**Fig. 3A**). Three candidate proteins were identified by mass spectrometry, including NKRF, heterogeneous nuclear ribonucleoprotein R (HNRNPR), and heterogeneous nuclear ribonucleoprotein M (HNRNPM; Supplementary Table S8). These proteins have been reported as transcriptional regulators (20–22). RNA pulldown assay and RNA-binding protein immunoprecipitation (RIP) analysis further validated that only NKRF could significantly enrich Uc003xsl.1 (**Fig. 3B** and **C**; Supplementary Fig. S3I). To further identify the NKRF-binding motif of Uc003xsl.1, a series of isoforms were constructed on the basis of the secondary structure of Uc003xsl.1 predicted by RNAfold (RNAfold webserver). The RNA pulldown assay showed that Uc003xsl.1 truncation containing nt 1,301–1,500 retained the similar capability to bind to NKRF as efficiently as the full-length Uc003xsl.1 (Supplementary Fig. S3J and S3K). When nt 1,301–1,500 was deleted from the full-length lncRNA, the truncated Uc003xsl.1 lost its capacity to bind to NKRF (Supplementary Fig. S3K).

To explore how Uc003xsl.1 regulated NFκB-responsive transcription, we first examined the levels of NKRF in MDA-MB-231-P3 and BT549 cells and found that neither Uc003xsl.1 knocking down nor overexpression could affect the mRNA or protein levels of NKRF (**Fig. 3D–F**). In addition, we explored whether the interaction between

(*Continued.*) **G,** TCGA and Genotype-Tissue Expression data showed that Uc003xsl.1 was upregulated in TNBC tissues ($n = 100$) compared with other subtype breast cancer tissues ($n = 759$). **H,** Uc003xsl.1 is highly expressed in MDA-MB-231-P3 cell and TNBC cell lines compared with other subtypes of breast epithelial cell lines, as measured by qRT-PCR. **I,** ISH analysis of Uc003xsl.1 expression in paraffin-embedded tumor sections of patients with TNBC ($n = 196$, cohort 2). Representative images of Uc003xsl.1 expression (brown) in normal adjacent tissues, primary TNBC with or without regional LN metastasis, and distant metastasis (Met). Scale bars, 50 μm. **J,** Uc003xsl.1 levels were significantly higher in patients with TNBC with positive LN metastasis and distant metastasis. **K,** Survival was analyzed and compared between patients with high (H-score >110, $n = 105$) and low (H-score ≤ 110, $n = 91$) levels of Uc003xsl.1 expression ($n = 196$, cohort 2). The cut-off values were the median expression of Uc003xsl.1 in TNBC tissues. **L,** Multivariable Cox proportional hazards analysis of prognostic variables was performed with patients with TNBC ($n = 196$, cohort 2). Error bars, SDs of three independent experiments. *, $P < 0.05$; **, $P < 0.01$; ***, $P < 0.001$.

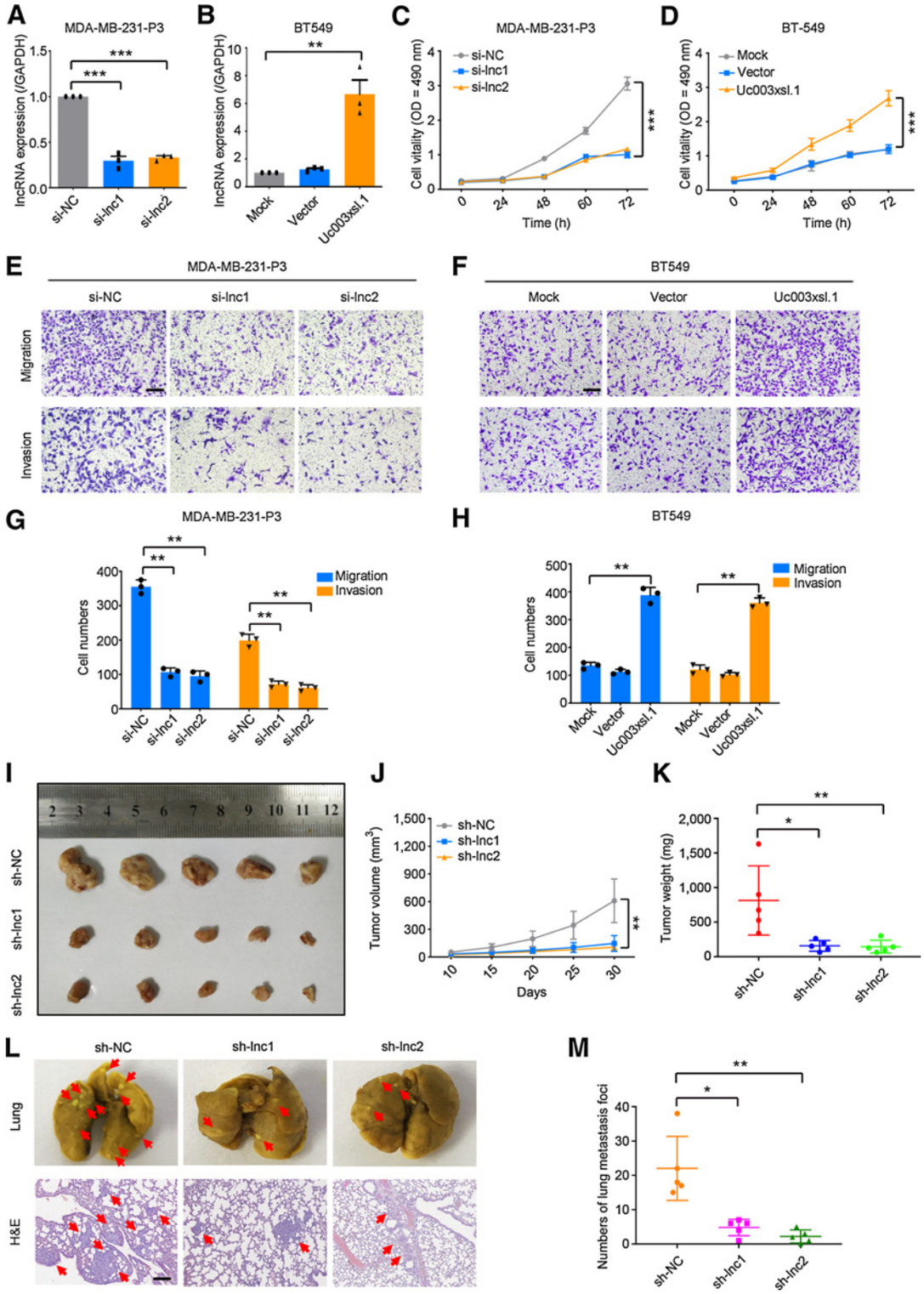

Figure 2.

Uc003xsl.1 promotes proliferation, migration, and invasion of TNBC cells. **A** and **B,** The efficiency of Uc003xsl.1 knockdown in MDA-MB-231-P3 cells (**A**) and overexpression in BT549 cells (**B**) was verified by qRT-PCR. **C** and **D,** Cell viability after Uc003xsl.1 knockdown in MDA-MB-231-P3 cells (**C**) and overexpression in BT549 cells (**D**) was assessed by MTS assays. **E–H,** Representative images and histogram analysis of transwell assays after Uc003xsl.1 knockdown in MDA-MB-231-P3 cells (**E** and **G**) and overexpression in BT549 cells (**F** and **H**). Scale bars, 100 μm. **I,** Gross appearance of xenograft tumors after subcutaneous injections with sh-NC, sh-lnc1, and sh-lnc2 groups ($n = 5$). **J** and **K,** Tumor volumes (**J**) and weights (**K**) were measured in the indicated groups ($n = 5$). **L,** Representative images of lung colonization and H&E staining of lung sections after injection of MDA-MB-231-P3 cells with sh-NC, sh-lnc1, and sh-lnc2 groups into tail veins of mice ($n = 5$). Scale bars, 100 μm. **M,** Histogram analysis for the number of metastatic foci representing lung metastasis ($n = 5$). Error bars, SDs of three independent experiments. *, $P < 0.05$; **, $P < 0.01$; ***, $P < 0.001$.

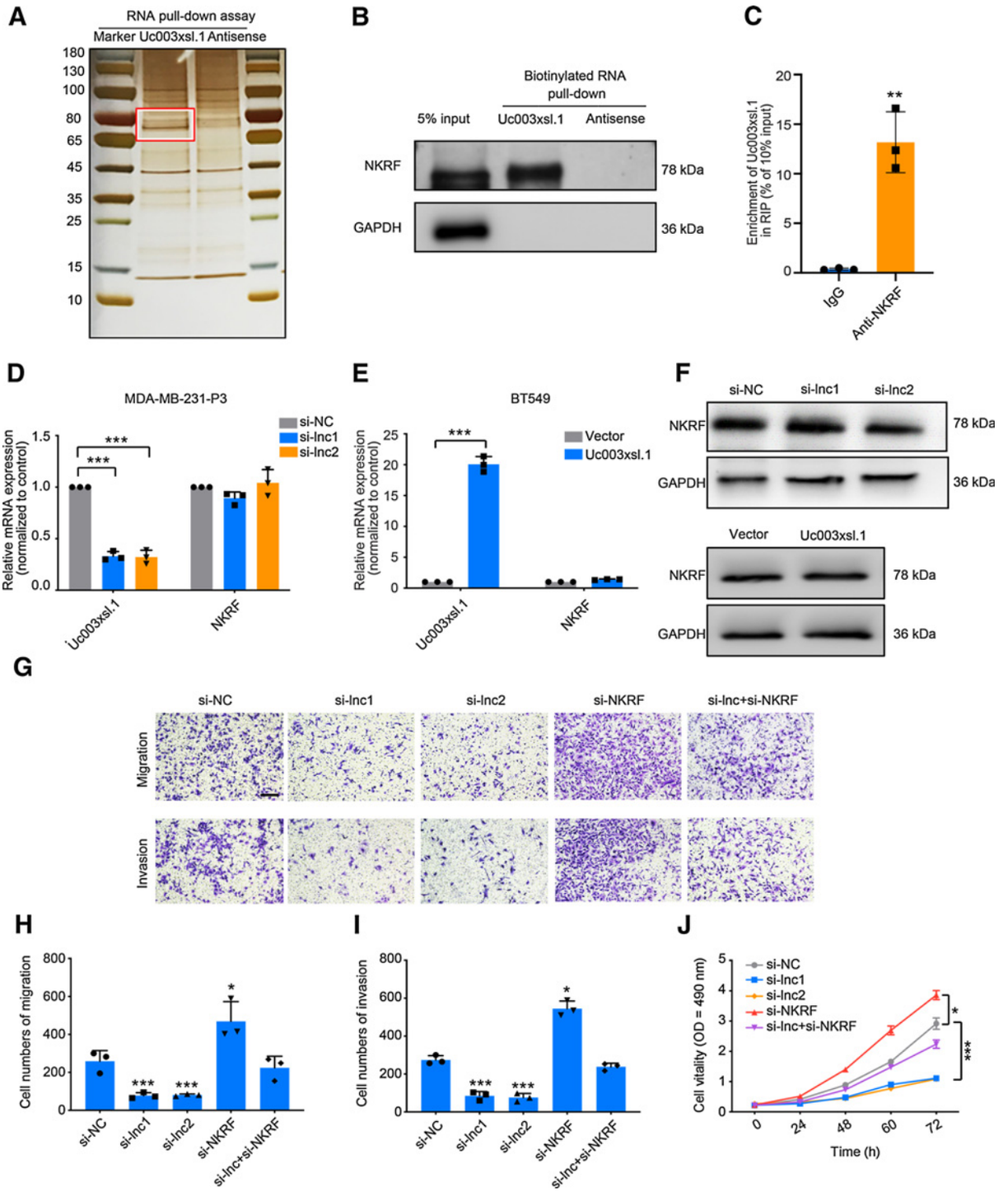

Figure 3.

Uc003xsl.1 interacts with NKRF to promote NFκB transcriptional activity–mediated TNBC cell migration and invasion. **A,** RNA pulldown assay of Uc003xsl.1, followed by electrophoresis and silver staining in MDA-MB-231-P3 cells. The band in the red frame was specifically precipitated by Uc003xsl.1 but not by antisense RNA submitted for mass spectrometric detection. **B,** Western blotting analysis of proteins from Uc003xsl.1 pulldown assays revealed that Uc003xsl.1 specifically interacts with NKRF. **C,** RIP assays revealed Uc003xsl.1 bound to NKRF. **D–F,** qRT-PCR (**D** and **E**) and Western blotting (**F**) analysis showed that neither Uc003xsl.1 knocking down in MDA-MB-231-P3 cells nor overexpression in BT549 cells could affect the mRNA or protein levels of NKRF. **G–J,** Representative images (**G**) and histogram analysis of migration assays (**H**), invasion assays (**I**), and MTS assays (**J**) revealed that depletion of NKRF partially reversed the effects of Uc003xsl.1-silencing MDA-MB-231 cells. Scale bars, 100 μm. Error bars represent SDs of three independent experiments. *, $P < 0.05$; **, $P < 0.01$; ***, $P < 0.001$.

Uc003xsl.1 and NKRF contributed to TNBC progression and found that abolishing the NKRF expression could rescue siUc003xsl.1-mediated inhibition of cell migration, invasion, and proliferation in MDA-MB-231-P3 cells (**Fig. 3G–J**), further supporting a key role of NKRF in Uc003xsl.1-mediated TNBC progression.

Uc003xsl.1 relieves the inhibitory effect of NKRF on NFκB-mediated IL8 transcription

NKRF has been implicated in the basal silencing of NFκB target genes by binding to the negative regulatory element (NRE) in promoters of these genes (23–25). Herein, we hypothesized that the Uc003xsl.1/NKRF complex is a key regulator of NFκB transcriptional activity. The luciferase reporter assay showed that total NFκB transcriptional activity was significantly inhibited when silencing Uc003xsl.1 and increased when silencing NKRF (Supplementary Fig. S3L). However, knockdown of Uc003xsl.1 and NKRF did not affect P65 phosphorylation (Supplementary Fig. S3M), suggesting that prolonged NFκB activation in TNBC cells is not a result of continuous P65 phosphorylation in the cytoplasm but might rely on the transcriptional modifications of P65 in the nucleus. These findings suggested that Uc003xsl.1/NKRF complex is involved in regulating NFκB-mediated transcriptional activity.

NFκB drives the expression of a series of genes (26). Next, we explored the NFκB-responsive transcription that was regulated by Uc003xsl.1/NKRF complex. The ChIP-seq was performed for NKRF in MDA-MB-231-P3 cells treated with si-Uc003xsl.1 or control siRNA. The ChIP-seq data displayed 3,604 peak calls in the control siRNA group (Supplementary Table S9A and S9B) and Uc003xsl.1 siRNA enhanced the NKRF occupancy in the DNA-binding regions (**Fig. 4A** and **B**) with 161 binding loci than that by the treatment of control siRNA (Supplementary Table S9C). Then the RNA-seq analysis was also performed on MDA-MB-231-P3 cells transfected with control or Uc003xsl.1 siRNA. A gene signature with highly significant expression changes post-Uc003xsl.1 siRNA treatment was observed (Supplementary Table S10). Integrative gene set enrichment analysis (GSEA) was used to analyze the RNA-seq and ChIP-seq data upon Uc003xsl.1 silencing and displayed a substantial subset of 374 genes ($\log_2$ fold-change > 2, FDR < 0.05) were regulated by Uc003xsl.1/NKRF axis (**Fig. 4C**; Supplementary Table S11). Then, the gene set containing 374 genes was analyzed by Kyoto Encyclopedia of Genes and Genomes (KEGG) enrichment and found that NFκB pathway was one of the most significantly regulated pathways ($P = 0.0126$), with six (6/374) NFκB target genes were identified (Supplementary Fig. S4A). These data argued that Uc003xsl.1 binding with NKRF enhanced the transcription of the subset of NFκB-responsive genes.

The KEGG analysis revealed that the cytokine–cytokine receptor interaction and NFκB signaling pathway were regulated by Uc003xsl.1, indicating NFκB-related cytokines may be the downstream mediators of Uc003xsl.1 in regulating TNBC progression (Supplementary Fig. S4A). Next, we compared the cytokine profiles of NFκB target genes in the supernatants, secreted by MDA-MB-231-P3 cells with or without siUc003xsl.1, using Luminex multiplex cytokine assays. The levels of 12 cytokines in the supernatants were significantly decreased in response to Uc003xsl.1 silencing ($P < 0.05$; **Fig. 4D**; Supplementary Table S12). With the intersection analysis of ChIP-seq, RNA-seq, and NFκB-related cytokine profiles, three NFκB-responsive cytokines were identified as follows: IL8 (IL8 was annotated in Supplementary Tables S9–S11 as CXCL8), IL1beta, and IL6 (**Fig. 4E**). Further analysis revealed that only IL8 mRNA and secreted protein levels, as well as its transcriptional activity, could be downregulated by siUc003xsl.1 and increased by siNKRF (**Fig. 4F–H**; Supplementary Fig. S4B and S4C). In addition, the silencing of NKRF expression affected the expression of IL8 via siUc003xsl.1 (**Fig. 4F–H**). Collectively, Uc003xsl.1 participated in regulating IL8 expression by preventing the repression of NKRF on NFκB-mediated transcription.

Furthermore, we assessed whether IL8 is the functional downstream mediator for Uc003xsl.1-mediated TNBC metastasis. Reportedly, high levels of IL8 expression were correlated with poor clinical outcomes in breast cancer (27). TCGA data revealed that patients with TNBC with high levels of IL8 expression showed a decline in DFS and OS compared with those with low levels of IL8 (Supplementary Fig. S4D and S4E). Strikingly, the knockdown of IL8 expression inhibited proliferation, migration, and invasion of MDA-MB-231-P3 cells *in vitro* and *in vivo* (Supplementary Fig. S5A–S5G), while treating MDA-MB-231-P3-siUc003xsl.1 cells with 3 ng/mL IL8 rescued the inhibitory effects of si-Uc003xsl.1 in cell migration and invasion (Supplementary Fig. S5H–S5J). In line with these observations, knockdown of Uc003xsl.1 in MDA-MB-468 cells also inhibited IL8 transcription and expression (Supplementary Fig. S6A–S6C). These results confirmed that the elevated expression of Uc003.xsl.1 in TNBC cells enhanced the malignant behaviors of tumor cells via regulating of NKRF/IL8 axis.

Uc003xsl.1 serves as a molecular decoy between NKRF and IL8 promoter

ChIP-seq analysis identified the potential NKRF enrichment locus in the IL8 promoter (**Fig. 5A**). The primers designed for the ChIP-PCR assay are listed in **Fig. 5A**. Both the ChIP-seq and ChIP-PCR assay revealed that knockdown of Uc003xsl.1 increased the accumulation of NKRF in IL8 promoter in MDA-MB-231-P3 cells (**Fig. 5B**; Supplementary Fig. S4F). Consistently, silencing of Uc003xsl.1 inhibited the enrichment of phosphorylated P65 in the IL8 promoters, whereas silencing of NKRF exerted an opposite effect (**Fig. 5C**). On the other hand, the elevated expression of Uc003xsl.1 in MDA-MB-231 cells and BT549 reduced NKRF binding to the IL8 promoter and facilitated IL8 transcription and expression similar to the level in MDA-MB-231-P3 cells (Supplementary Fig. S6D–S6L). These results confirmed that the elevated expression of Uc003.xsl.1 in MDA-MB-231-P3 cells enhanced the malignant phenotypes of TNBC cells by regulating NKRF/IL8 axis.

lncRNAs function as decoy modules that mimic or compete with their consensus DNA-binding motifs of specific transcription factors to regulate the related transcription (28). Therefore, we hypothesized that the direct binding of Uc003xsl.1 with NKRF prevents its binding to the IL8 promoter, thereby abolishing NKRF repression to P65-mediated IL8 transcription. To validate this hypothesis, the binding domain of NKRF with Uc003xsl.1 was investigated examined using a series of NKRF-truncated mutants in MDA-MB-231 and BT549 cells. NKRF comprises 705 amino acids in its primary structure, with three conservative domains in the C-terminus, including DSRM, G-patch, and R3H. Therefore, three fragments, NKRF-D1 (1–250 aa), NKRF-D2 (200–450 aa), and NKRF-D3 (400–705 aa), were used (**Fig. 5D**). The RIP-PCR assay revealed that the fragment of NKRF-D3 (400–705 aa) retained the binding ability with Uc003xsl.1 (**Fig. 5E**; Supplementary Fig. S7A). Then, NKRF-D3 was further divided into three fragments, NKRF3-D1, NKRF3-D2, and NKRF3-D3, which contain the conservative domains of DSRM, G-patch, and R3H, respectively (**Fig. 5D**). The RIP assay showed that NKRF3-D3 containing R3H retained the binding ability with Uc003xsl.1; when the R3H domain was deleted from NKRF, the mutant (NKRF-DR3H) abolished the binding ability with Uc003xsl.1 (**Fig. 5F**; Supplementary Fig. S7A).

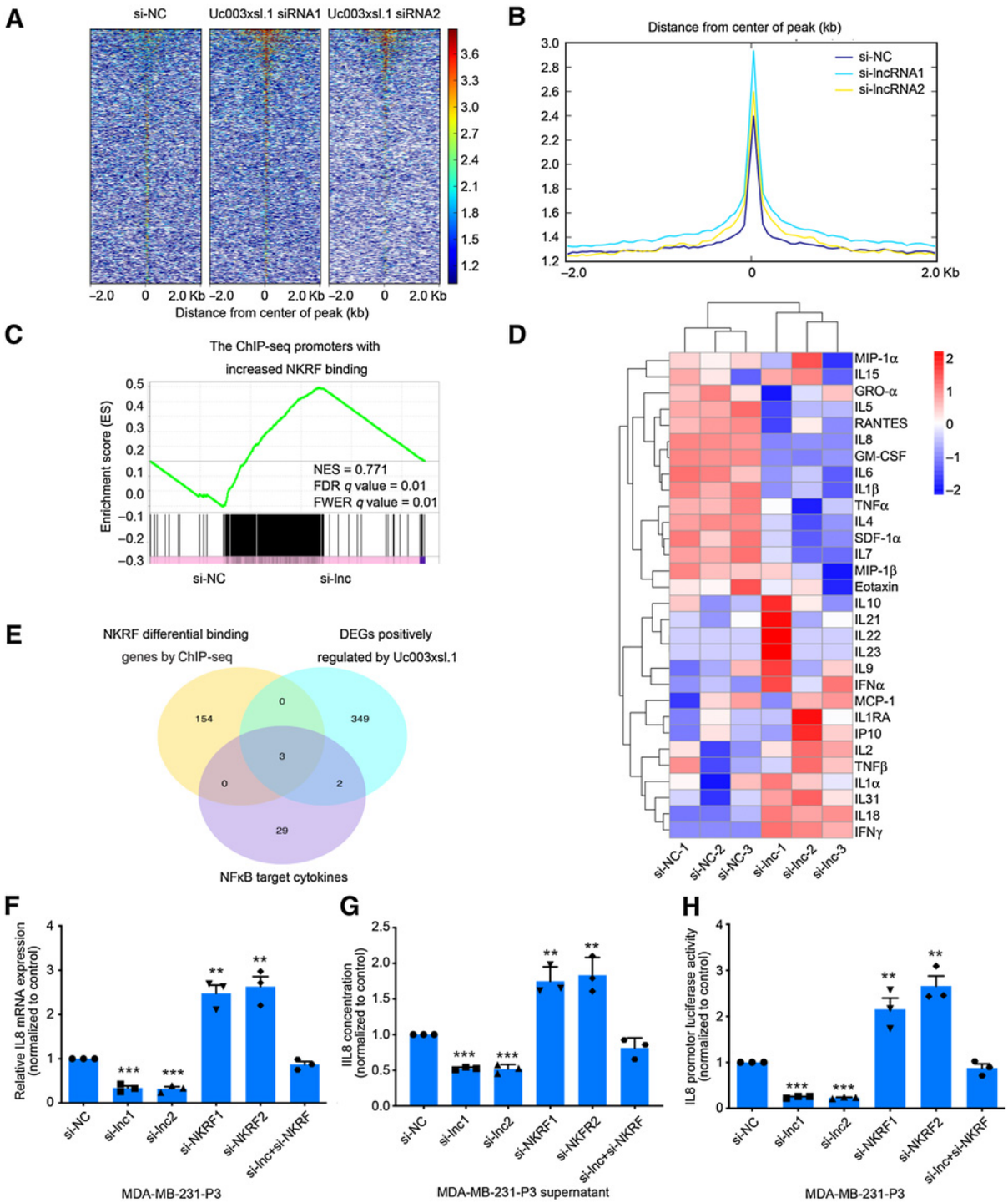

Figure 4.

The Uc003xsl.1/NKRF complex promotes NFκB target gene (*IL8*) transcription in TNBC cells. **A** and **B,** Heatmaps (**A**) and peaks (**B**) of NKRF genomic binding at the target sites in MDA-MB-231-P3 cells after the transduction of control or Uc003xsl.1 siRNA. A 2-kbp interval centered on the NKRF peak was shown. **C,** GSEA showed the enrichment of ChIP-seq promoter peaks with a significant increase in NKRF binding for the downregulated genes in MDA-MB-231-P3 cells after transfection of Uc003xsl.1 siRNA compared with si-NC. FDR, false discovery rate; FWER, family-wise error rate; NES, normalized enrichment score. **D,** Heatmap analysis displayed NFκB-regulated cytokine profiles in supernatants secreted by MDA-MB-231-P3 and Uc003xsl.1-depleted MDA-MB-231-P3 by Luminex multiplex cytokine assays. **E,** Venn diagram revealed intersection genes of the ChIP-seq, RNA-seq, and NFκB-regulated cytokine profiles in MDA-MB-231-P3 cells after transfection of Uc003xsl.1 siRNA and control siRNA. DEG, differentially expressed genes. **F–H,** IL8 mRNA levels (**F**), concentration in supernatants (**G**), and transcriptional activity (**H**) were respectively assessed by qRT-PCR, ELISA, and luciferase assay in MDA-MB-231-P3 cells after transfection of control siRNA, Uc003xsl.1 siRNA, NKRF siRNA, or both Uc003xsl.1 siRNA and NKRF siRNA. Error bars, SDs of three independent experiments. **, $P < 0.01$; ***, $P < 0.001$.

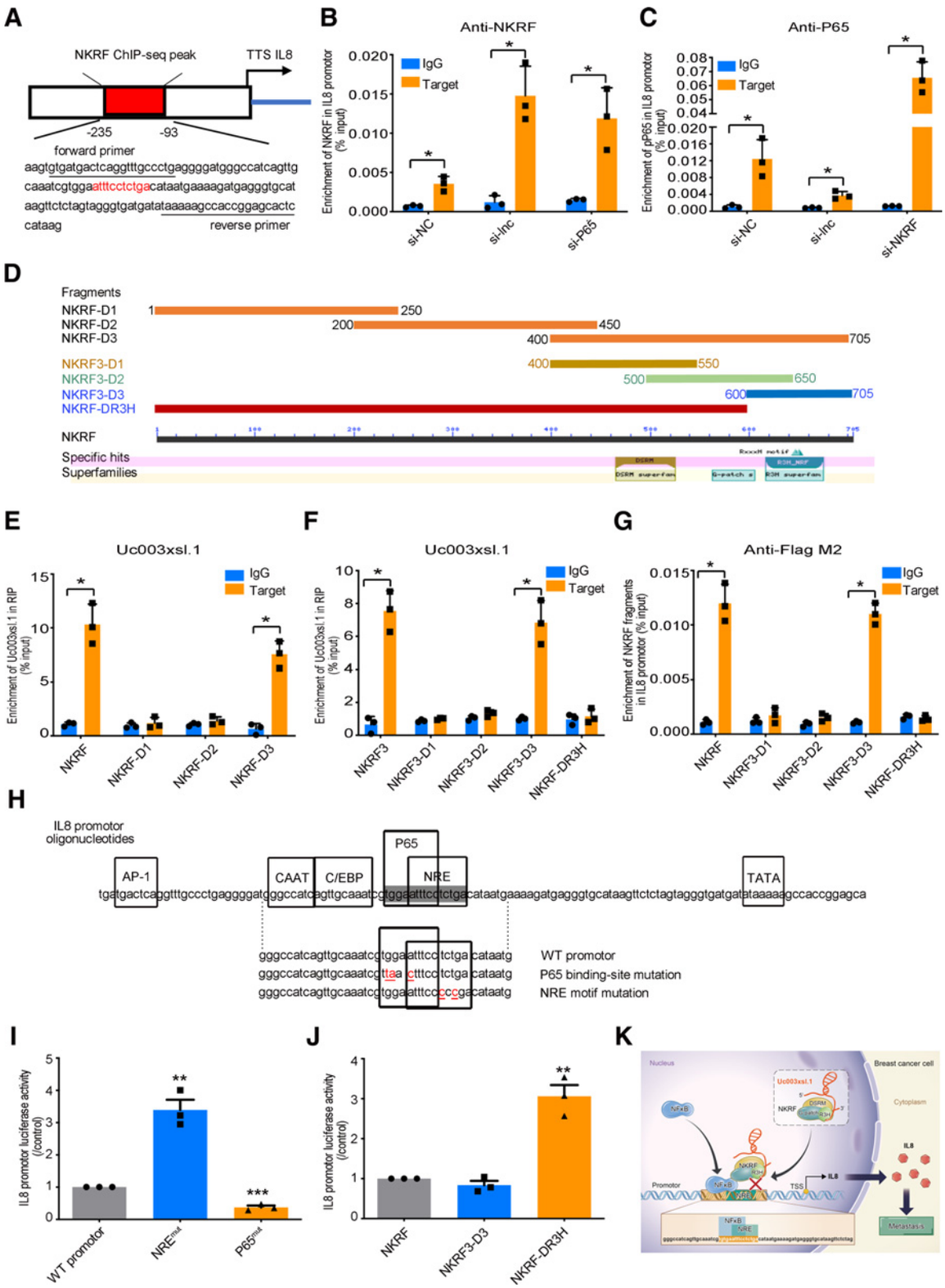
A
NKRF ChIP-seq peak
TTS IL8
-235
-93
forward primer
aagtgtgatgactcaggtttgccctgaggggatgggccatcagttg
caaatcgtggaatttcctctgacataatgaaaagatgagggtgcat
aagttctctagtagggtgatgatataaaaagccaccggagcactc
cataag
reverse primer
B
Anti-NKRF
IgG
Target
Enrichment of NKRF in IL8 promotor (% input)
si-NC
si-Inc
si-P65
C
Anti-P65
IgG
Target
Enrichment of pP65 in IL8 promotor (% input)
si-NC
si-Inc
si-NKRF
D
Fragments
NKRF-D1
NKRF-D2
NKRF-D3
NKRF3-D1
NKRF3-D2
NKRF3-D3
NKRF-DR3H
NKRF
Specific hits
Superfamilies
E
Uc003xsl.1
IgG
Target
Enrichment of Uc003xsl.1 in RIP (% input)
NKRF
NKRF-D1
NKRF-D2
NKRF-D3
F
Uc003xsl.1
IgG
Target
Enrichment of Uc003xsl.1 in RIP (% input)
NKRF3
NKRF3-D1
NKRF3-D2
NKRF3-D3
NKRF-DR3H
G
Anti-Flag M2
IgG
Target
Enrichment of NKRF fragments in IL8 promotor (% input)
NKRF
NKRF3-D1
NKRF3-D2
NKRF3-D3
NKRF-DR3H
H
IL8 promotor oligonucleotides
AP-1
CAAT
C/EBP
P65
NRE
TATA
tgatgactcaggtttgccctgaggggatgggccatcagttgcaaatcgtggaatttcctctgacataatgaaaagatgagggtgcataagttctctagtagggtgatgatataaaaagccaccggagca
gggccatcagttgcaaatcgtggaatttcctctgacataatg
WT promotor
gggccatcagttgcaaatcgttaactttcctctgacataatg
P65 binding-site mutation
gggccatcagttgcaaatcgtggaatttccccgacataatg
NRE motif mutation
I
IL8 promotor luciferase activity (/control)
WT promotor
NRE^mut
P65^mut
J
IL8 promotor luciferase activity (/control)
NKRF
NKRF3-D3
NKRF-DR3H
K
Nucleus
Breast cancer cell
Cytoplasm
Uc003xsl.1
NKRF
DSRM
NFκB
IL8
Promotor
TSS
NRE
Metastasis

These results demonstrated that Uc003xsl.1 predominately interacts with the R3H domain of NKRF.

NKRF reportedly represses NFκB transcriptional activities via binding to the NRE in the promoters of NFκB-responsive genes to prevent the binding of P65 with these promoters (23, 24). Next, we identified whether NKRF binds with the NRE element of the IL8 promoter via its R3H domain. The ChIP assay revealed that NKRF3-D3 could be enriched in the IL8 promoter in MDA-MB-231 and BT549 cells; in addition, the mutant (NKRF-DR3H) could not bind to the IL8 promoter (**Fig. 5G**; Supplementary Fig. S7B). To further analyze the role of NRE for IL8 transcription, parallel experiments were carried out with the wild-type (WT) promoter or promoters with mutations in the NFκB-binding motif or NRE element (**Fig. 5H**). The mutations in NRE reduce the binding of NKRF and dismiss the repression of NRE to IL8 transcription (29). Similarly, mutations in the P65-binding motif inactivated the NFκB-binding subunit (30), decreasing IL8 transcription. These mutants in the IL8 promoter were used for luciferase reporter assay in MDA-MB-231. The NRE motif mutation (NRE^{mut}) in the IL8 promoter led to increased transcriptional activity, whereas IL8 promoter transcriptional activity was significantly reduced when the NFκB-binding site was mutated ($P65^{mut}$; **Fig. 5I**), suggesting that NRE is the critical negative regulatory motif for IL8 transcription. Herein, we have shown that the binding of NKRF to Uc003xsl.1 relies on its R3H domain. Next, we delineated the involvement of the R3H domain of NKRF for NRE-dependent negative regulation of IL8 transcription. The WT NKRF or NKRF-DR3H was used to test the IL8 promoter activity by luciferase reporter assay in MDA-MB-231. IL8 promoter activity was elevated when the R3H domain was deleted from NKRF (**Fig. 5J**). Collectively, the current results indicated that the R3H domain of NKRF is the docking site for both Uc003xsl.1 and the NRE element of the IL8 promoter. The docking of Uc003xsl.1 on the R3H domain of NKRF prevents the binding of NKRF on the NRE element of the IL8 promoter and enhances IL8 transcription (**Fig. 5K**).

We have demonstrated that Uc003xsl.1 truncation containing nt 1,301–1,500 retained the capability to bind to NKRF as efficiently as the full-length Uc003xsl.1 (Supplementary Fig. S3J and S3K). We further address whether the fragment of nt 1,301–1,500 mimics the action of the full-length Uc003xsl.1 to regulate the NFκB/IL8 axis. The ChIP-PCR analysis revealed that nt 1,301–1,500 fragment (Uc003xsl.1-T fragment) and full-length Uc003xsl.1 could equally reduce the binding of NKRF to IL8 promoter and boost IL8 expression; however, the ΔT fragment deleted nt 1,301–1,500 from Uc003xsl.1 lost the ability to prevent NKRF binding to the IL8 promoter and thus could not increase IL8 expression in MDA-MB-231 cells (Supplementary Fig. S7C–S7F). These results demonstrated that Uc003xsl.1 could directly bind to NKRF through nt 1,301–1,500, and the fragment of nt 1,301–1,500 could behave similarly as the full-length Uc003xsl.1.

Trop2-targeting, reduction-responsive NP-mediated systemic delivery of Uc003xsl.1 siRNA to inhibit Uc003xsl.1-induced TNBC metastasis

Because the upregulation of Uc003xsl.1 could activate NFκB to promote TNBC metastasis, systemic delivery of siRNA to silence Uc003xsl.1 expression could be an effective strategy to inhibit TNBC metastasis. However, siRNAs are easily eliminated by serum nucleases and are unable to penetrate the cell membrane. Therefore, efficient delivery vehicles are needed for siRNA delivery. NPs are promising tools for systemic siRNA delivery, and several RNAi NP platforms have been entered early-phase clinical trials for cancer treatment (31, 32). Particularly, because tumor tissues show distinguishing microenvironment compared with normal tissues (e.g., weakly acidic and hypoxia environment), stimuli-responsive NPs have been recently developed as effective siRNA delivery systems, which can respond to tumor microenvironment stimuli to achieve efficient intracellular siRNA delivery and better anticancer effect (33, 34). In this study, we employed the reduction-responsive NP platform to transport Uc003xsl.1 siRNA (siUc003xsl.1) to evaluate the influence of Uc003xsl.1 silencing on the metastasis of TNBC. Trop-2 is a membrane located glycoprotein and is overexpressed in many epithelial cancers, including TNBCs (35). Anti-Trop-2 antibody–drug conjugate sacituzumab govitecan (IMMU-132) has been developed to treat metastatic TNBCs (36). Thus, the anti-Trop-2 antibody was conjugated to the surface of the reduction-responsive NPs, which is expected to improve the TNBC-targeting ability of the resulting siRNA delivery system.

First, we examined the Trop2 expression in TNBC cells and found that Trop2 was highly expressed in highly metastatic MDA-MB-231-P3 cells and TNBC cells than other subtype breast cancer cells (**Fig. 6A**). Consistently, Trop2 showed higher expression in TNBC tissues compared with normal breast tissues and other subtype tissues (Supplementary Fig. S8A and S8B). The immunofluorescence assay indicated the membrane and cytoplasmic location of Trop2 in TNBC cells (**Fig. 6B**). These results demonstrated that Trop2 was highly expressed in TNBC and could be used as a potential target for TNBC-specific siRNA delivery and targeted TNBC therapy.

Next, we encapsulated siUc003xsl.1 into the reduction-responsive NP platform that composed of a solid poly (disulfide amide; PDSA)/cationic lipid core and a lipid-poly (ethylene glycol; lipid-PEG) shell and subsequently conjugated the anti-Trop2 mAb to the surface of siRNA loaded NPs via the reaction between Trop2 antibody and the *N*-hydroxysuccinimide ester group of lipid-PEG (**Fig. 6C**). As shown in **Fig. 6D–G**, the resulting NPs (denoted Trop2 NPs) exhibit a uniform spherical morphology with an average size of approximately 70 nm. Compared with the NPs without Trop2 antibody conjugation, the Trop2 NPs showed a better Uc003xsl.1 silencing, and > 80% of

Figure 5.

Uc003xsl.1 serves as a molecular decoy between NKRF and IL8. **A,** Schematic images of IL8 promoter. The red frame displays the potential region of NKRF enrichment in the IL8 promoter by ChIP-seq analysis, and the specific primers for following ChIP-PCR analysis are underlined. **B** and **C,** ChIP-PCR analyzed NKRF enrichment (**B**) and P65 enrichment (**C**) in the IL8 promoter in MDA-MB-231-P3 cells after transfection of control siRNA, Uc003xsl.1 siRNA, P65 siRNA, and NKRF siRNA. **D,** Fragments and conserved domains of NKRF protein. **E** and **F,** RIP assays identified that the NKRF3-D3 fragment specifically binds to Uc003xsl.1 in MDA-MB-231 cells. **G,** ChIP-PCR analysis revealed that the NKRF3-D3 fragment binds to the IL8 promoter but not the NKRF-DR3H in MDA-MB-231 cells. **H,** The sequence of the IL8 promoter. Identified binding sites for transcription factors are illustrated (23). Shown is the sequence of oligonucleotides of IL8 promoter WT, P65 mutant, and NRE mutant. Point mutations are underlined. The P65-binding site and NRE are shaded. **I,** IL8 promoter luciferase activity was detected in MDA-MB-231 cells after transfection of luciferase reporter plasmids containing the IL8 promoter WT, or versions carrying mutations in the NRE (NRE^{mut}) or P65-binding site ($P65^{mut}$). **J,** IL8 promoter luciferase activity was assessed in MDA-MB-231 cells after cotransfection of luciferase reporter vector containing the WT IL8 promoter and NKRF expression vectors, with or without R3H domain. **K,** The schematic working model of Uc003xsl.1 overexpression drives the NKRF/NFκB/IL8 axis in TNBC. Uc003xsl.1 upregulated in TNBC could bind to R3H domain of NKRF and directly masks the binding motif of R3H with NRE in NFκB-responsive gene (*IL8*) promoter, thereby abolishing NKRF repression to IL8 transcriptional activity and finally promoting NFκB/IL8-mediated TNBC metastasis. Error bars, SDs of three independent experiments. *, $P < 0.05$; **, $P < 0.01$; ***, $P < 0.001$.

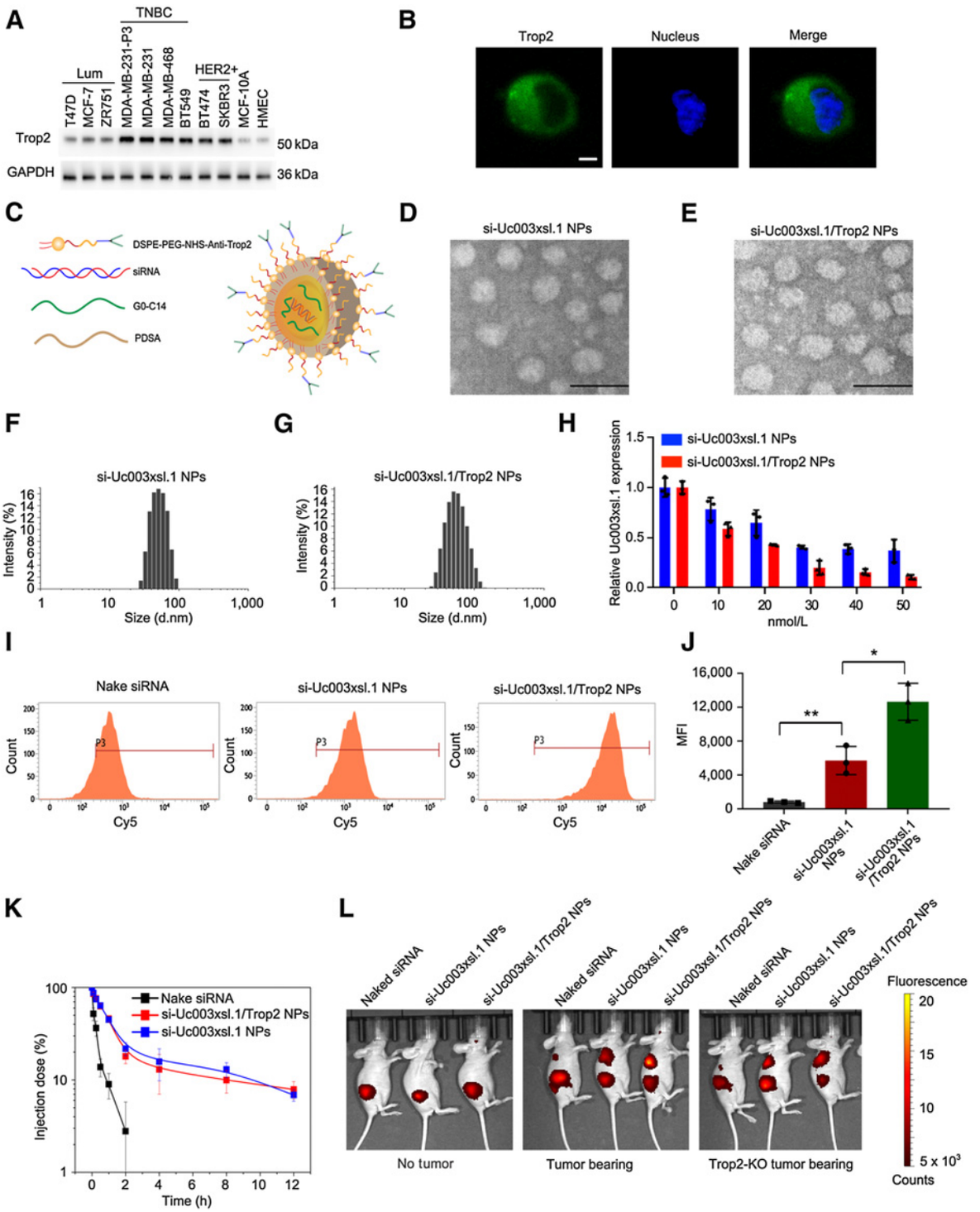

Figure 6.

Synthesis and characterization of siUc003xsl.1/Trop2 NPs. **A,** Western blotting analysis showed that Trop2 was highly expressed in MDA-MB-231-P3 cells and TNBC cells. **B,** Immunofluorescence analysis indicated the membrane and cytoplasmic location of Trop2 in MDA-MB-231 cells. **C,** Schematic illustration of the components of si-Uc003xsl.1/Trop2 NPs: PDSA polymer, lipid-PEG (1,2-distearoyl-sn-glycero-3-phospho-ethanolamine-N-[methoxy(polyethylene glycol)-3000]), DSP E-PEG$_{3k}$ linked with Anti-Trop2 antibody, and cationic lipid G0-C14. **D** and **E,** Morphology of the si-Uc003xsl.1 NPs (**D**) and the si-Uc003xsl.1/Trop2 NPs (**E**). Scale bars, 100 nm. **F** and **G,** Size distribution of si-Uc003xsl.1 NPs (**F**) and si-Uc003xsl.1/Trop2 NPs (**G**). **H,** Uc003xsl.1 expression level detected by qRT-PCR in MDA-MB-231-P3 cells treated with the si-Uc003xsl.1 NPs or si-Uc003xsl.1/Trop2 NPs at different siRNA doses. **I** and **J,** Flow cytometry profile (**I**) and mean fluorescence intensity (MFI; **J**) of MDA-MB-231-P3 cells incubated with Cy5-labeled naked siRNA, si-Uc003xsl.1 NPs, and si-Uc003xsl.1/Trop2 NPs at 37°C for 4 hours at a 1 nmol/L siRNA dose. **K,** Blood circulation profile of the naked siRNA, si-Uc003xsl.1 NPs, and si-Uc003xsl.1/Trop2 NPs. **L,** Overlaid fluorescent image of the nude mice, MDA-MB-231-P3 tumor-bearing mice, and MDA-MB-231-P3-Trop2-KO tumor-bearing mice at 24 hours after injection of the formulas in **K**. Error bars, SDs of three independent experiments. *, $P < 0.05$; **, $P < 0.01$.

Uc003xsl.1 expression could be suppressed at a siRNA dose of 30 nmol/L (**Fig. 6H**). To demonstrate that the better gene silencing of the Trop2 NPs is attributed to the more cellular uptake of siRNA mediated by Trop2 antibody, we labeled siUc003xsl.1 with the fluorescent dye Cy5 and then examined the siRNA uptake using flow cytometry. As expected, the MDA-MB-231 cells showed around 2-fold stronger uptake of the Trop2 NPs compared with the NPs without Trop2 antibody conjugation (**Fig. 6I** and **J**). This result strongly demonstrates that the incorporation of Trop2 antibody improves the gene silencing efficacy of Uc003xsl.1 in TNBC cells.

We further examined their pharmacokinetics and biodistribution (BioD) of the Trop2 NPs. Pharmacokinetics was evaluated by intravenous injection of naked siUc003xsl.1, siUc003xsl.1 NPs and siUc003xsl.1/Trop2 NPs into healthy mice (1 nmol of siRNA dose per mouse, $n = 3$), respectively. As shown in **Fig. 6K**, the encapsulation of siUc003xsl.1 into NPs could dramatically enhance its blood circulation. However, there is no significant difference in the blood circulation ability for the siRNA-loaded NPs with or without Trop2 antibody conjugation, and both showed a half-time ($t_{1/2}$) of approximately 4 hours. BioD was examined by intravenous injection of the cy5-siUc003xsl.1 loaded NPs in nude mice, tumor-bearing mice, and Trop2-KO tumor-bearing mice. The tumors and major organs were harvested for BioD quantification 24 hours post-injection. Because of the presence of Trop2 antibody-mediated tumor-targeting ability, the Trop2 NPs exhibited much stronger tumor accumulation than naked siUc003xsl.1 and the NPs without antibody conjugation in tumor-bearing mice but displayed a similar tumor accumulation as siUc003xsl.1 NPs did in Trop2-KO tumor-bearing mice (**Fig. 6L**; Supplementary Fig. S8C–S8E).

We finally investigated whether the Trop2 NPs could silence Uc003xsl.1 expression *in vivo* and suppress tumor growth and metastasis. We constructed a subcutaneous xenograft tumor model using MDA-MB-231-P3 cells or MDA-MB-231-P3-Trop2 KO cells (**Fig. 7A**) and then intravenously injected the PBS, scramble-control siRNA NPs, siUc003xsl.1 NPs, and siUc003xsl.1/Trop2 NPs into the tumor-bearing mice every 2 days at a 1 nmol siRNA dose per mouse ($n = 3$) for three consecutive injections by tail vein (**Fig. 7A**). Within a long evaluation period of 30 days after the last injection, the Trop2 NPs showed the strongest ability to inhibit the tumor growth compared with other treatment formulas in MDA-MB-231-P3 tumor-bearing mice but displayed a similar inhibitory effect on tumor growth as siUc003xsl.1 NPs did in Trop2-KO tumor-bearing mice (**Fig. 7B** and **C**). To examine the ability of the Trop2 NPs to suppress TNBC metastasis, we further established a lung metastatic model using (Luc)-MDA-MB-231-P3 cells or (Luc)-MDA-MB-231-P3-Trop2-KO cells (**Fig. 7D**). After 7 weeks of tumor cell injection via tail vein, lung metastasis loci were detected by bioluminescence imaging (**Fig. 7E**). Then, three consecutive intravenous injections of PBS, scramble-control siRNA NPs, siUc003xsl.1 NPs, and siUc003xsl.1/Trop2 NPs were administered via tail vein (1 nmol of siRNA dose per mouse, $n = 3$). As shown in **Fig. 7E–G**, at 21 days post-injection, the Trop2 NPs showed the strongest ability to reduce the metastatic tumor burden in MDA-MB-231-P3 tumor-bearing mice but showed a moderate effect similarly as siUc003xsl.1 NPs did in Trop2-KO tumor-bearing mice. The results of ISH and IHC staining further confirmed that the administration of the Trop2 NPs was the most effective treatment in inhibiting tumor growth and metastasis, as demonstrated by low Uc003xsl.1 expression (ISH), less proliferation (Ki67), and less amount of micrometastasis detected in the lung tissues (H&E; Supplementary Fig. S8F–S8J). These data demonstrated that Trop2-targeting NPs could enhance the therapeutic effect of targeting Uc003xsl.1 against TNBC tumor growth and metastasis.

To evaluate the *in vivo* toxicity of the Trop2 NPs, healthy mice were intravenously injected with the Trop2 NPs (1 nmol siRNA dose per mouse, $n = 3$) once every day. After three consecutive injections, no histologic toxicity was detected in the heart, liver, spleen, lung, and kidney (Supplementary Fig. S9A). In addition, multiple hematologic parameters, including aspartate aminotransferase, alanine aminotransferase, albumin, alkaline phosphatase, creatinine, and total protein range were in the normal range (Supplementary Fig. S9B). These results indicated good biocompatibility of the siRNA delivery NP platform used in this study.

Discussion

Effective therapies for breast cancer metastasis, especially TNBC, are yet an urgent clinical requirement. NFκB is aberrantly activated in various cancers, including TNBC, and is essential for tumor development and recurrence (37). However, the mechanism underlying the activation of NFκB-mediated transcription in cancer cells remains obscure. Recent evidence indicates that lncRNAs are associated with aberrant activation of NFκB in tumors (38, 39). We have previously reported that a cytoplasmic lncRNA NKILA binds to NFκB/IκB complex, and directly masks the IKK phosphorylating sites, thereby preventing IKK-induced IκB phosphorylation in breast cancer (18). Different from the most previously identified NFκB regulators that either affect the amount of IκB or regulate NFκB/IκB phosphorylation (18, 39). Here we explored that a novel nuclear lncRNA Uc003xsl.1 could directly bind to the R3H domain of NFκB-repressing factor, NKRF. And we also found that R3H domain of NKRF is responsible for NRE binding in the IL8 promoter to prevent NFκB-mediated IL8 transcription subsequently. Therefore, the binding of Uc003xsl.1 with NKRF prevents NKRF from binding to the NRE of NFκB-responsive promoters, including promoter of IL8 gene and thus, enhancing NFκB transcriptional activity and IL8 transcription. Moreover, 160 additional NKRF-binding locations were altered upon siUc003xsl.1, such as EZH2 and TRIM3. On the other hand, Uc003xsl.1 also influences the expression of 435 additional genes independent of NKRF binding based on the RNA-seq data, such as ANXA family genes and IGF2BP2. These genes have been discovered to play roles in cancer development (40–43). Whether and how genes are involved in Uc003xsl.1 mediated TNBC tumorigenesis should be pursued in the future.

In addition, we identified IL8 as the downstream effector of Uc003xsl.1. IL8 is the typical target for classical NFκB signaling (44). Reportedly, IL8 serum concentration correlates with the tumor burden of patients and with a poor prognosis of the disease (45). IL8 derived from tumors is critical for establishing a tumor microenvironment that attracts myeloid-derived suppressor cells (MDSC), facilitating the tumor to evade the immune system (46). In addition to the effects on MDSCs, IL8 retains dendritic cells in the tumor in a disorienting manner that eventually decreases the antitumor immunity (47, 48). Therefore, IL8 could be a multifaceted inflammatory mediator used by the tumor to drive malignant progression simultaneously. Herein, we discovered that Uc003xsl.1 persistent activation of NFκB/IL8 axis is essential to promote TNBC progression. Moreover, the prolonged NFκB/IL8 activation is not a result of continuous IKK or IκB phosphorylation but relies on the translational modification of P65 repressor, NKRF. Thus, the identification of Uc003xsl.1 affects the prediction of cancer progression and the development of novel antitumor

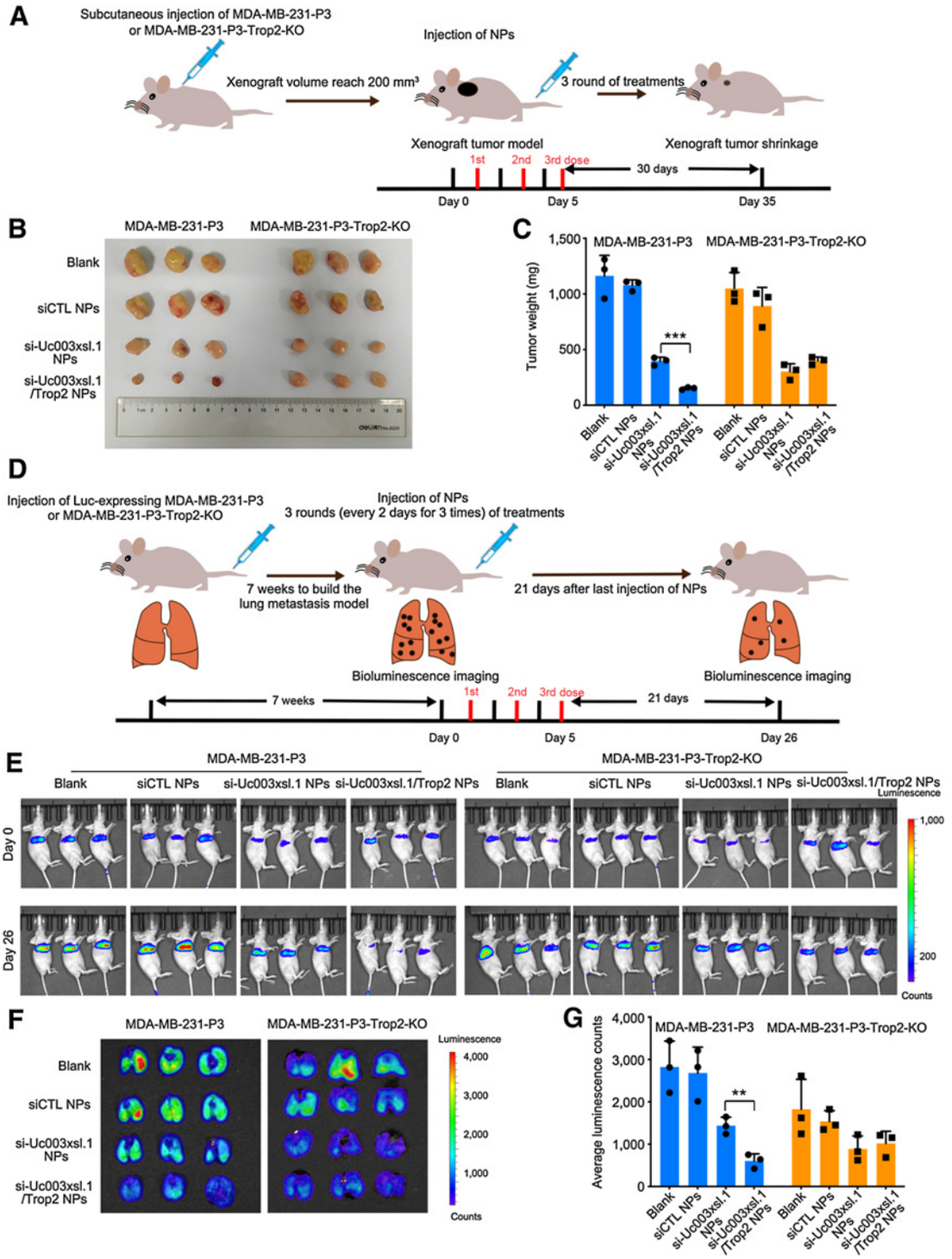

Figure 7.

Reduction-responsive, NP-targeting, Trop2-mediated Uc003xsl.1 silencing synergistically reverses TNBC progression *in vivo*. **A,** Schematic illustration of tumor inoculation and various treatments in the MDA-MB-231-P3 or MDA-MB-231-P3-Trop2-KO tumor-bearing nude mice. After the xenograft volume reached 200 mm^3, mice were intravenously injected with PBS (Blank), scramble-control siRNA NPs, siUc003xsl.1 NPs or siUc003xsl.1/Trop2 NPs at a 1 nmol siRNA dose per mouse once every 2 days for 3 times. Tumors were harvested at indicated days after injection. **B** and **C,** Image of collected tumors (**B**) and tumor weight (**C**) of the tumor-bearing nude mice treated with the formulas in **A**. **D,** Schematic illustration of tumor inoculation and various treatments in the Luc-MDA-MB-231-P3 and Luc-MDA-MB-231-P3-Trop2-KO metastatic tumor-bearing nude mice. Seven weeks after tumor inoculation, mice were treated with the formulas in **A**. **E,** Bioluminescence images of lung metastatic tumor-bearing nude mice at days 0 and 26. **F** and **G,** Bioluminescence images and histogram analysis of metastatic tumor tissues in lungs collected from Luc-MDA-MB-231-P3 and Luc-MDA-MB-231-P3-Trop2-KO metastatic tumor-bearing nude mice at the endpoint (day 26). Error bars, SDs of three independent experiments. **, $P < 0.01$; ***, $P < 0.001$.

strategies. Besides IL8, the cytokine profiling demonstrated significant changes in IFNγ, GMCSF, IL7, IL4, IL6, IL1β, and IL5. Interestingly, these cytokines have been revealed to participate in cancer progression in other studies (14, 15). Thus, whether and how these cytokines are involved in Uc003xsl.1-mediated TNBC progression needs to be investigated further.

Several functional lncRNAs were showed anticancer effects in cell lines or animal models. Nonetheless, few efforts have been made to explore effective *in vivo* regulation strategies to improve therapeutic outcomes. Herein, we developed a reduction-responsive NP to transport Uc003xsl.1 siRNAs to evaluate the therapeutic potency of metastatic TNBC. The reduction-responsive NP platform consisted of multi-disulfide bond-containing PDSA polymers that could rapidly respond to the high GSH concentration in tumor cells (32, 49), which has been reported to accelerate intracellular siRNA release and boost gene silencing in our previous study. We also observed that Trop2 is overexpressed on the TNBC cell membrane. Several preclinical and clinical studies (NCT04152499, NCT04601285) of Trop2-drug conjugates displayed impressive therapeutic outcomes in breast cancers as well as other solid tumors (35). To improve the TNBC-targeting ability of siUc003xsl.1 NP delivery system, we generated the antibody-NPs conjugate by conjugation of the anti-Trop2 mAb to the surface of the reduction-responsive NPs. In the xenograft and metastatic tumor models, the Trop2-targeting reduction-responsive RNAi NP platform can effectively suppress tumor growth and metastasis and shows the following features and benefits: (i) long blood circulation and high tumor accumulation; (ii) specific-targeting TNBC cells; (iii) nontoxicity and biodegradation.

In conclusion, our findings showed that lncRNA Uc003xsl.1, upregulated in human TNBC tissues, acted as an oncogene and significantly boosted TNBC progression. Uc003xsl.1 was deemed a molecular decoy binding to the R3H domain of NKRF, which prevented NKRF binding to the NRE motif of NFκB-responsive gene promoter, especially the IL8 promoter, thereby eliminating NKRF repression of NFκB transcriptional activity, promoting IL8 transcription, and inducing IL8-mediated tumor metastasis. Thus, the systematic delivery of Uc003xsl.1 siRNA by applying Trop2-linked redox-responsive NP provides a promising strategy for TNBC treatment.

Authors' Disclosures

No disclosures were reported.

Authors' Contributions

Y. Xu: Conceptualization, resources, data curation, formal analysis, supervision, funding acquisition, validation, investigation, methodology, writing–original draft, writing–review and editing. **W. Ren:** Conceptualization, data curation, formal analysis, validation, investigation, methodology, writing–original draft. **Q. Li:** Formal analysis, investigation, methodology, writing–original draft. **C. Duan:** Resources, formal analysis, investigation, methodology. **X. Lin:** Resources, investigation, methodology. **Z. Bi:** Investigation. **K. You:** Investigation. **Q. Hu:** Resources, investigation. **N. Xie:** Resources, investigation. **Y. Yu:** Formal analysis, investigation. **X. Xu:** Conceptualization, resources, formal analysis, investigation, writing–review and editing. **H. Hu:** Conceptualization, resources, supervision, investigation, writing–review and editing. **H. Yao:** Conceptualization, resources, supervision, funding acquisition, investigation, writing–review and editing.

Acknowledgments

This study was supported by the National Science and Technology Major Project (2020ZX09201021), to H. Yao; the National Natural Science Foundation of China, project 81972471 to H. Yao and 81730077, 82025026 to H. Hu; the Guangdong Basic and Applied Basic Research Foundation, project 2020A1515010115 to Y. Xu and 2019A1515110082 to X. Lin; the Guangdong province Science and Technology Plan Foundation (A2019259), to Y. Xu; the Guangzhou Science and Technology Major Program (201704020131), the Guangdong Science and Technology Department (2017B030314026), the Sun Yat-sen University Clinical Research 5010 Program (2018007), the Sun Yat-sen Clinical Research Cultivating Program (SYS-C-201801), and the Medical Artificial Intelligence Project of Sun Yat-sen Memorial Hospital (YXRGZN201902), to H. Yao; the China Postdoctoral Science Foundation (2020TQ0377), to Q. Li.

The costs of publication of this article were defrayed in part by the payment of page charges. This article must therefore be hereby marked *advertisement* in accordance with 18 U.S.C. Section 1734 solely to indicate this fact.

Received May 12, 2021; revised October 14, 2021; accepted December 27, 2021; published first December 29, 2021.

References

1. Torre LA, Bray F, Siegel RL, Ferlay J, Lortet-Tieulent J, Jemal A. Global cancer statistics, 2012. CA Cancer J Clin 2015;65:87–108.
2. Foulkes WD, Smith IE, Reis-Filho JS. Triple-negative breast cancer. N Engl J Med 2010;363:1938–48.
3. Schmitt AM, Chang HY. Long noncoding RNAs in cancer pathways. Cancer Cell 2016;29:452–63.
4. Zhang Y, Pitchiaya S, Cieslik M, Niknafs YS, Tien JC, Hosono Y, et al. Analysis of the androgen receptor-regulated lncRNA landscape identifies a role for ARLNC1 in prostate cancer progression. Nat Genet 2018;50:814–24.
5. Dorji T, Monti V, Fellegara G, Gabba S, Grazioli V, Repetti E, et al. Gain of hTERC: a genetic marker of malignancy in oral potentially malignant lesions. Hum Pathol 2015;46:1275–81.
6. Lee S, Kopp F, Chang TC, Sataluri A, Chen B, Sivakumar S, et al. Noncoding RNA NORAD regulates genomic stability by sequestering PUMILIO proteins. Cell 2016;164:69–80.
7. Huang F, Chen W, Peng J, Li Y, Zhuang Y, Zhu Z, et al. LncRNA PVT1 triggers Cyto-protective autophagy and promotes pancreatic ductal adenocarcinoma development via the miR-20a-5p/ULK1 axis. Mol Cancer 2018;17:98.
8. Zhang E, Han L, Yin D, He X, Hong L, Si X, et al. H3K27 acetylation activated-long noncoding RNA CCAT1 affects cell proliferation and migration by regulating SPRY4 and HOXB13 expression in esophageal squamous cell carcinoma. Nucleic Acids Res 2017;45:3086–101.
9. Schmitz KM, Mayer C, Postepska A, Grummt I. Interaction of noncoding RNA with the rDNA promoter mediates recruitment of DNMT3b and silencing of rRNA genes. Genes Dev 2010;24:2264–9.
10. Chu C, Zhang QC, da Rocha ST, Flynn RA, Bharadwaj M, Calabrese JM, et al. Systematic discovery of Xist RNA binding proteins. Cell 2015;161:404–16.
11. McHugh CA, Chen CK, Chow A, Surka CF, Tran C, McDonel P, et al. The Xist lncRNA interacts directly with SHARP to silence transcription through HDAC3. Nature 2015;521:232–6.
12. Tay Y, Rinn J, Pandolfi PP. The multilayered complexity of ceRNA crosstalk and competition. Nature 2014;505:344–52.
13. Smale ST. Hierarchies of NF-kappaB target-gene regulation. Nat Immunol 2011;12:689–94.
14. Chaturvedi MM, Sung B, Yadav VR, Kannappan R, Aggarwal BB. NF-kappaB addiction and its role in cancer: 'one size does not fit all'. Oncogene 2011;30:1615–30.
15. Fornier MN, Rathkopf D, Shah M, Patil S, O'Reilly E, Tse AN, et al. Phase I dose-finding study of weekly docetaxel followed by flavopiridol for patients with advanced solid tumors. Clin Cancer Res 2007;13:5841–6.
16. Staudt LM. Oncogenic activation of NF-kappaB. Cold Spring Harb Perspect Biol 2010;2:a000109.
17. Karin M. NF-kappaB as a critical link between inflammation and cancer. Cold Spring Harb Perspect Biol 2009;1:a000141.
18. Liu B, Sun L, Liu Q, Gong C, Yao Y, Lv X, et al. A cytoplasmic NF-kappaB interacting long noncoding RNA blocks IkappaB phosphorylation and suppresses breast cancer metastasis. Cancer Cell 2015;27:370–81.
19. Zhang A, Zhao JC, Kim J, Fong KW, Yang YA, Chakravarti D, et al. LncRNA HOTAIR enhances the androgen-receptor-mediated transcriptional program and drives castration-resistant prostate cancer. Cell Rep 2015;13:209–21.

20. Nourbakhsh M, Hauser H. Constitutive silencing of IFN-beta promoter is mediated by NRF (NF-kappaB-repressing factor), a nuclear inhibitor of NF-kappaB. EMBO J 1999;18:6415–25.
21. Castrignanò T, Rizzi R, Talamo IG, De Meo PD, Anselmo A, Bonizzoni P, et al. ASPIC: a web resource for alternative splicing prediction and transcript isoforms characterization. Nucleic Acids Res 2006;34:W440–3.
22. Hu X, Harvey SE, Zheng R, Lyu J, Grzeskowiak CL, Powell E, et al. The RNA-binding protein AKAP8 suppresses tumor metastasis by antagonizing EMT-associated alternative splicing. Nat Commun 2020;11:486.
23. Nourbakhsh M, Kalble S, Dorrie A, Hauser H, Resch K, Kracht M. The NF-kappa b repressing factor is involved in basal repression and interleukin (IL)-1-induced activation of IL-8 transcription by binding to a conserved NF-kappa b-flanking sequence element. J Biol Chem 2001;276:4501–8.
24. Feng X, Guo Z, Nourbakhsh M, Hauser H, Ganster R, Shao L, et al. Identification of a negative response element in the human inducible nitric-oxide synthase (hiNOS) promoter: The role of NF-kappa B-repressing factor (NRF) in basal repression of the hiNOS gene. Proc Nat Acad Sci U S A 2002;99:14212–7.
25. Lu Z, Li Y, Takwi A, Li B, Zhang J, Conklin DJ, et al. miR-301a as an NF-κB activator in pancreatic cancer cells. EMBO J 2011;30:57–67.
26. Taniguchi K, Karin M. NF-κB, inflammation, immunity and cancer: coming of age. Nat Rev Immunol 2018;18:309–24.
27. Xing F, Liu Y, Sharma S, Wu K, Chan MD, Lo HW, et al. Activation of the c-Met pathway mobilizes an inflammatory network in the brain microenvironment to promote brain metastasis of breast cancer. Cancer Res 2016;76:4970–80.
28. Wang K, Jin W, Song Y, Fei X. LncRNA RP11-436H11.5, functioning as a competitive endogenous RNA, upregulates BCL-W expression by sponging miR-335-5p and promotes proliferation and invasion in renal cell carcinoma. Mol Cancer 2017;16:166.
29. Nourbakhsh M, Hoffmann K, Hauser H. Interferon-beta promoters contain a DNA element that acts as a position-independent silencer on the NF-kappaB site. EMBO J 1993;12:451–9.
30. Wu GD, Lai EJ, Huang N, Wen X. Oct-1 and CCAAT/enhancer-binding protein (C/EBP) bind to overlapping elements within the interleukin-8 promoter. The role of Oct-1 as a transcriptional repressor. J Biol Chem 1997;272:2396–403.
31. Whitehead KA, Langer R, Anderson DG. Knocking down barriers: advances in siRNA delivery. Nat Rev Drug Discov 2009;8:129–38.
32. Davis ME, Zuckerman JE, Choi CH, Seligson D, Tolcher A, Alabi CA, et al. Evidence of RNAi in humans from systemically administered siRNA via targeted nanoparticles. Nature 2010;464:1067–70.
33. Li Q, Qin T, Bi Z, Hong H, Ding L, Chen J, et al. Rac1 activates non-oxidative pentose phosphate pathway to induce chemoresistance of breast cancer. Nat Commun 2020;11:1456.
34. Bi Z, Li Q, Dinglin X, Xu Y, You K, Hong H, et al. Nanoparticles (NPs)-meditated LncRNA AFAP1-AS1 silencing to block Wnt/β-catenin signaling pathway for synergistic reversal of radioresistance and effective cancer radiotherapy. Adv Sci 2020;7:2000915.
35. Shvartsur A, Bonavida B. Trop2 and its overexpression in cancers: regulation and clinical/therapeutic implications. Genes Cancer 2015;6:84–105.
36. Bardia A, Mayer IA, Diamond JR, Moroose RL, Isakoff SJ, Starodub AN, et al. Efficacy and safety of anti-Trop-2 antibody drug conjugate sacituzumab govitecan (IMMU-132) in heavily pretreated patients with metastatic triple-negative breast cancer. J Clin Oncol 2017;35:2141–8.
37. Zhang Q, Lenardo MJ, Baltimore D. 30 years of NF-κB: a blossoming of relevance to human pathobiology. Cell 2017;168:37–57.
38. Xie C, Zhang LZ, Chen ZL, Zhong WJ, Fang JH, Zhu Y, et al. A hMTR4-PDIA3P1-miR-125/124-TRAF6 regulatory axis and its function in NF kappa B signaling and chemoresistance. Hepatology 2020;71:1660–77.
39. Ren X, Chen C, Luo Y, Liu M, Li Y, Zheng S, et al. lncRNA-PLACT1 sustains activation of NF-κB pathway through a positive feedback loop with IκBα/E2F1 axis in pancreatic cancer. Mol Cancer 2020;19:35.
40. Wan L, Xu K, Wei Y, Zhang J, Han T, Fry C, et al. Phosphorylation of EZH2 by AMPK suppresses PRC2 methyltransferase activity and oncogenic function. Mol Cell 2018;69:279–91.
41. Ji CH, Kim HY, Heo AJ, Lee SH, Lee MJ, Kim SB, et al. The N-Degron pathway mediates ER-phagy. Mol Cell 2019;75:1058–72.
42. Mousavian Z, Nowzari-Dalini A, Stam RW, Rahmatallah Y, Masoudi-Nejad A. Network-based expression analysis reveals key genes related to glucocorticoid resistance in infant acute lymphoblastic leukemia. Cell Oncol 2017;40:33–45.
43. Peng F, Xu J, Cui B, Liang Q, Zeng S, He B, et al. Oncogenic AURKA-enhanced N(6)-methyladenosine modification increases DROSHA mRNA stability to transactivate STC1 in breast cancer stem-like cells. Cell Res 2021;31:345–61.
44. Chow MT, Luster AD. Chemokines in cancer. Cancer Immunol Res 2014;2:1125–31.
45. Sanmamed MF, Perez-Gracia JL, Schalper KA, Fusco JP, Gonzalez A, Rodriguez-Ruiz ME, et al. Changes in serum interleukin-8 (IL-8) levels reflect and predict response to anti-PD-1 treatment in melanoma and non-small-cell lung cancer patients. Ann Oncol 2017;28:1988–95.
46. Alfaro C, Sanmamed MF, Rodríguez-Ruiz ME, Teijeira Á, Oñate C, González Á, et al. Interleukin-8 in cancer pathogenesis, treatment and follow-up. Cancer Treat Rev 2017;60:24–31.
47. Yousefi S, Stojkov D, Germic N, Simon D, Wang X, Benarafa C, et al. Untangling "NETosis" from NETs. Eur J Immunol 2019;49:221–7.
48. Gonzalez-Aparicio M, Alfaro C. Influence of Interleukin-8 and Neutrophil Extracellular Trap (NET) formation in the tumor microenvironment: is there a pathogenic role? J Immunol Res 2019;2019:6252138.
49. Xu X, Wu J, Liu S, Saw PE, Tao W, Li Y, et al. Redox-responsive nanoparticle-mediated systemic RNAi for effective cancer therapy. Small 2018;14:e1802565.